ELSEVIER

Journal of Neuroscience Methods xxx (2005) xxx–xxx

JOURNAL OF NEUROSCIENCE METHODS

www.elsevier.com/locate/jneumeth

Magnetic resonance imaging at 9.4 T as a tool for studying neural anatomy in non-vertebrates

Catherine K. Brinkley [a], Nancy H. Kolodny [b], Susan J. Kohler [c], David C. Sandeman [a], Barbara S. Beltz [a,*]

[a] *Department of Biological Sciences, 106 Central Street, Wellesley College, Wellesley, MA 02481, USA*
[b] *Department of Chemistry, Wellesley College, Wellesley, MA 02481, USA*
[c] *General Electric Healthcare, Waukesha, WI 53188, USA*

Received 16 September 2004; received in revised form 2 February 2005; accepted 2 February 2005

Abstract

This report describes magnetic resonance imaging (MRI) methods we have developed at 9.4 T for observing internal organs and the nervous system of an invertebrate organism, the crayfish, *Cherax destructor*. We have compared results acquired using two different pulse sequences, and have tested manganese (Mn^{2+}) as an agent to enhance contrast of neural tissues in this organism. These techniques serve as a foundation for further development of functional MRI and neural tract-tracing methods in non-vertebrate systems.

Keywords: Crustacea; MRI; Brain; Nervous system; Crayfish; Manganese

1. Introduction

Classical anatomical methods have been used for centuries to resolve the structural and functional relationships between and within organs and tissues of animals. These methods require sacrifice of the subject and preservation of the tissues by fixation, often followed by sectioning and treatment with histological stains in order to provide resolving power and contrast between tissue types. These techniques are laborious and depend on the reconstruction of serial sections in order to visualize the three-dimensional architecture of a structure. In contrast, magnetic resonance imaging (MRI) provides a window through which to view a living, functioning organism at the organ and tissue levels, without killing the subject or performing arduous reconstructions. MRI thereby allows relatively rapid imaging of specimens and the opportunity to repeatedly examine the same individual in longitudinal studies. The goal of the present study was to develop MR imaging and contrast-enhancement methods in a non-vertebrate model system, in order to lay a foundation for development of tract-tracing and functional imaging techniques that can be used for basic research in these organisms.

While MRI has become a relatively commonplace clinical approach for examining soft tissues, it has only recently been exploited in non-vertebrate animal research (Brinkley et al., 2004; Herberholz et al., 2004; Michaelis et al., 2005). Invertebrate animals present significant advantages over vertebrates for MR imaging because they do not require anesthetics, can be easily immobilized, and can stay in the magnet for many hours. This allows multiple studies, either to follow dynamic processes or to use a variety of pulse sequences, some of long duration, to elucidate different features of the animal's anatomy. Furthermore, use of a small bore, high field magnet with strong magnetic field gradients provides excellent sensitivity and resolution of anatomical structures.

We have used the Australian crayfish, *Cherax destructor*, as our model because it is a hardy creature adapted to terrestrial environments, where water may be scarce and can survive periods out of the water, unlike many crustacean species (e.g., lobsters and crabs) that are also popular neurobiological models. This is key to the animal's suitability for MRI study where the animal is out of the water for many hours during imaging. In addition, *C. destructor* is an excellent model for

* Corresponding author. Tel.: +1 781 283 3048; fax: +1 781 283 3642.
E-mail address: bbeltz@wellesley.edu (B.S. Beltz).

0165-0270/$ – see front matter © 2005 Elsevier B.V. All rights reserved.
doi:10.1016/j.jneumeth.2005.02.003

MRI studies because it will remain motionless in small, dark spaces, such as the MRI probe, for several hours and has no respiratory movements.

Introduction of the paramagnetic contrast agent Mn^{2+} into the blood system of the crayfish can enhance visualization of neural tissues. Mn^{2+} has a long history of use in MRI for enhancement of contrast in brain and other tissues in vertebrate organisms (Aoki et al., 2002; Burnett et al., 1984; Cory et al., 1987; Fornasiero et al., 1987; Geraldes et al., 1986; Leergaard et al., 2003; Lin and Koretsky, 1997; London et al., 1989; Newland et al., 1987; Pautler and Koretsky, 2002; Pautler et al., 1998; Tjälve et al., 1995, 1996; Watanabe et al., 2001; Van der Linden et al., 2002), but its use is just emerging in invertebrate organisms (Brinkley et al., 2004; Herberholz et al., 2004; Michaelis et al., 2005). Mn^{2+} is especially useful as a contrast agent in living tissues because it has an ionic radius and charge similar to calcium (Ca^{2+}), and can therefore substitute for Ca^{2+} in many biological systems (Hunter et al., 1980). It is known that Mn^{2+} is taken up by neural tissue of the related crustacean *Nephrops norvegicus* at six times the exposure concentration, in hemolymph at three times the exposure concentration, and in muscle tissue at only half the exposure concentration (Baden and Neil, 1998). Therefore, as neural tissue sequesters disproportionately more Mn^{2+} relative to other tissues, Mn^{2+} can be used as a contrast agent in MRI applications where neural tissue is the primary focus. Because *C. destructor* does not require anesthetics, there are no non-specific regions of activity as seen in studies that use light anesthesia, and there is no reduction of activity as seen in studies with heavy anesthesia (Aoki et al., 2002). Additional bonuses for contrast agent studies of the nervous system in *C. destructor* are that there is no blood brain barrier (Abbott, 1971, 1972) and the arterial vasculature is closed (Sandeman, 1967), ensuring delivery of contrast agents directly to the brain and neural tissues without artificial disruption.

In this report, we compare images of various tissue types acquired using two different pulse sequences and test Mn^{2+}-enhancement methods for visualizing neural tissues. These studies serve as a foundation for the development of MRI methods for use in neural tract-tracing and functional MRI applications.

2. Materials and methods

2.1. Crayfish preparation

C. destructor (4–5 cm carapace length) were used in these studies. The large claws were removed at their bases so that larger animals would fit into the 30 mm inner diameter MRI probe, and also to reduce artifacts due to movement. For claw removal, the claw was squeezed until the animal autotomised the limb, so that the valve in the blood vessel to the limb closed reflexively (McVean, 1982). Claws were regenerated by the animals over the next molt period.

Mn^{2+} was injected into the pericardium of crayfish in the form of an aqueous solution of $MnCl_2$ (Sigma, St. Louis, MO), which dissociates into ions at neutral pH. The $MnCl_2$ solution was diluted with crayfish physiological saline (205 mmol l^{-1} NaCl, 5.4 mmol l^{-1} KCl, 10.2 mmol l^{-1} $CaCl_2$, 1.2 mmol l^{-1} $MgCl_2$, 2.4 mmol l^{-1} $NaHCO_3$, pH 7.4) to the desired concentration. Injections (40 μl/cm carapace length) of several concentrations of $MnCl_2$ (1, 10, 120 mM and 1 M) were tested; 120 mM resulted in images with good contrast; injection of the 1 M solution was lethal. After $MnCl_2$ injection, the animal's physical activity decreased, as evidenced by reduced tail flipping. However, there were no obvious long-term detrimental effects as individual crayfish survived as many as three sequential injections over a period of months, and survived up to 1 year after the initial injection.

2.2. MRI

Crayfish were imaged within 15 min of $MnCl_2$ administration using a Bruker Avance DRX 400 MHz NMR spectrometer with a 9.4 T vertical wide bore magnet, actively shielded gradients of 2.4 G/(cm A) with a maximum field of 96 G/cm (Bruker Biospin, Ettlingen, Germany), and were kept in the

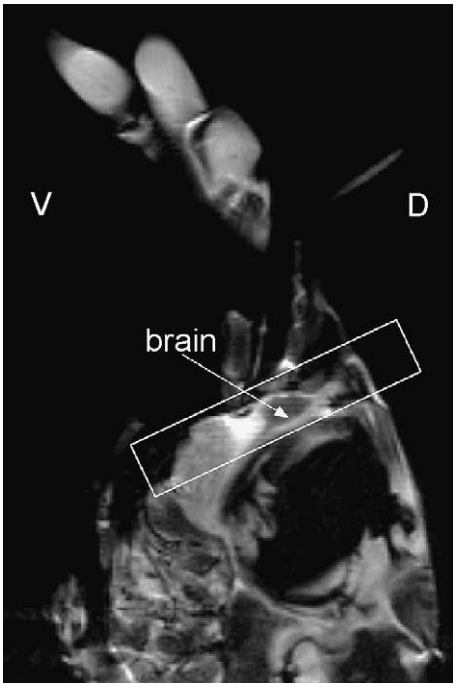

Fig. 1. Lateral view of the cephalothorax of *C. destructor* from a scout T2-weighted (RARE) image of the crayfish in one of three orthogonal planes showing orientation of slice selection for brain imaging over the area that contains the brain, eyestalks and esophageal connectives (ventral (V), dorsal (D)). A claw can be seen near the top of the image. Slices were aligned with the exoskeleton lying beneath the brain. This image was produced using RARE_BIO (FOV 4 cm, MTX 256, SLTH 1.0 mm, N_{avg} 1, TR 3112.5 ms, TE 60.8 ms, TA 1.39 min).

magnet at 20 °C for up to 12 h without adverse effects. Animals were wrapped in Parafilm (Pechniney Plastic Packaging, Chicago, IL) to reduce movement and placed in a Corning® plastic tube. The tube was then placed into the 30 mm birdcage volume coil (Bruker Instruments, Billerica, MA) of the MRI probe. The probe was inserted into the vertical bore magnet and MR images were acquired at 20 °C. Several pulse sequences were tested, with and without prior Mn^{2+} injection (see Section 3).

Scout images were produced using the Bruker ParaVision tripilot pulse sequence, a RARE (fast spin echo) sequence that creates three perpendicular images [field of view (FOV) 4 cm, matrix (MTX) 256, slice thickness (SLTH) 1.0 mm, number of repetitions (N_{avg}) 1, repetition time (TR) 3112.5 ms, echo time (TE) 60.8 ms, acquisition time (TA) 1.39 min]. Using the scout images, MRI slices of ensuing images were aligned in the plane of the ventral surface of the head (Fig. 1). In order to align the plane of the MRI scans symmetrically through the small brain (∼14 mm^3 in crayfish of 4–5 cm carapace length), the imaging plane was adjusted until the esophageal connectives appeared to be the same length.

Multi-slice spin echo and rapid acquisition relaxation-enhanced (fast spin echo) pulse sequences were used for the production of T1- and T2-weighted images, respectively. Depending on the size of the animal, in-plane resolution ranged from 102 to 113 μm in each dimension. Slice thickness ranged from 300 to 500 μm. Sagittal sections were produced using the Bruker ParaVision RARE_BIO T2-weighted sequence [MTX 256, TE 46.0 or 67.5 ms; FOV, SLTH, N_{avg}, TA and TR varied for different animals, with TR (∼3000–5000 ms) dependent on the number of slices] and the MSME_BIO T1-weighted sequence [MTX 256, TE 10.2 ms; FOV, SLTH, N_{avg}, TA and TR (300–1543 ms) varied for different animals] without Mn^{2+} injection. After injection of $MnCl_2$, T1- and T2-weighted images were compared and further analyses were done using the T1-weighted protocol. TA ranged from minutes to 1 or 2 h. To determine the clearance time of the Mn^{2+}, animals were imaged on sequential days for between 1 and 9 days post-$MnCl_2$ administration. Mn^{2+} contrast enhancement was no longer evident on the fourth day following $MnCl_2$ administration.

2.3. Gross anatomy

In order to verify structures seen with MRI, a crayfish with a carapace length of 3 cm was fixed for 2 weeks in Bouin's fixative (75 ml saturated aqueous picric acid, 25 ml concentrated formalin, 5 ml glacial acetic acid; Humason, 1979). Sections (1–2 mm thickness) were cut with a razor in the same plane as the MR images (e.g., Fig. 4b) and examined. Slices were photographed with a Spot Diagnostic camera (Spot Diagnostic Instruments Inc., Sterling Heights, MI) attached to a Nikon SMZ-10A microscope.

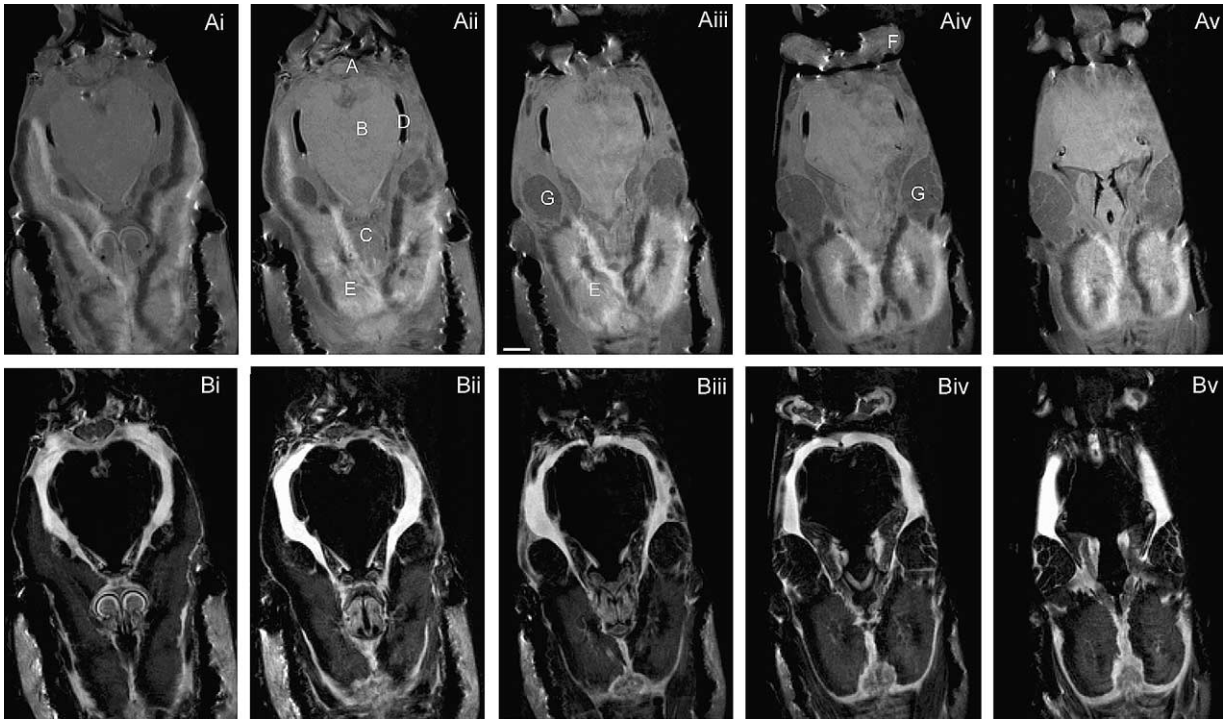

Fig. 2. Comparison of anatomical features revealed in T1-weighted (MSME; top) and T2-weighted (RARE; bottom) images of alternate sections 500 μm apart through the animal in the horizontal plane, slices 500 μm thick with in-plane resolution 125 μm × 125 μm. MSME parameters: FOV 3.2 cm, MTX 256, N_{avg} 4, TR 1543 ms, TE 10.2 ms, TA 26.2 min; RARE parameters: FOV 3.2 cm, MTX 256, N_{avg} 4, TR 7580 ms, TE 67.5 ms, TA 16.1 min. A, brain; B, stomach; C, gastric mill; D, blood sinus; E, hepatopancreas; F, eye; G, muscle. Scale bar in (Aiii) = 2 mm.

3. Results

Slices through the cephalothorax of an individual crayfish (Fig. 2) illustrate that in the absence of Mn^{2+} the two pulse protocols enhance different tissue types. For instance, in the images produced with the T2-weighted pulse sequence (Fig. 2Bi–Bv, lower row of images), the neural tissue and stomach appear dark while the gastric mill is brighter than the neural tissue and its tissue organization is readily distinguishable. The T1-weighted images (Fig. 2Ai–Av, upper row of images) show no contrast between the neural tissue and the stomach, but both tissues are brighter than in the T2-weighted images. Hepatopancreas is clearly visualized in the T1-weighted slices, but is barely visible in the T2-weighted images. On the other hand, the T2-weighted sequence produces better contrast in the eyestalk than the T1-weighted sequence. Details of the stomach and pylorus are clearly visualized using the T1-weighted sequence, but appear as dark

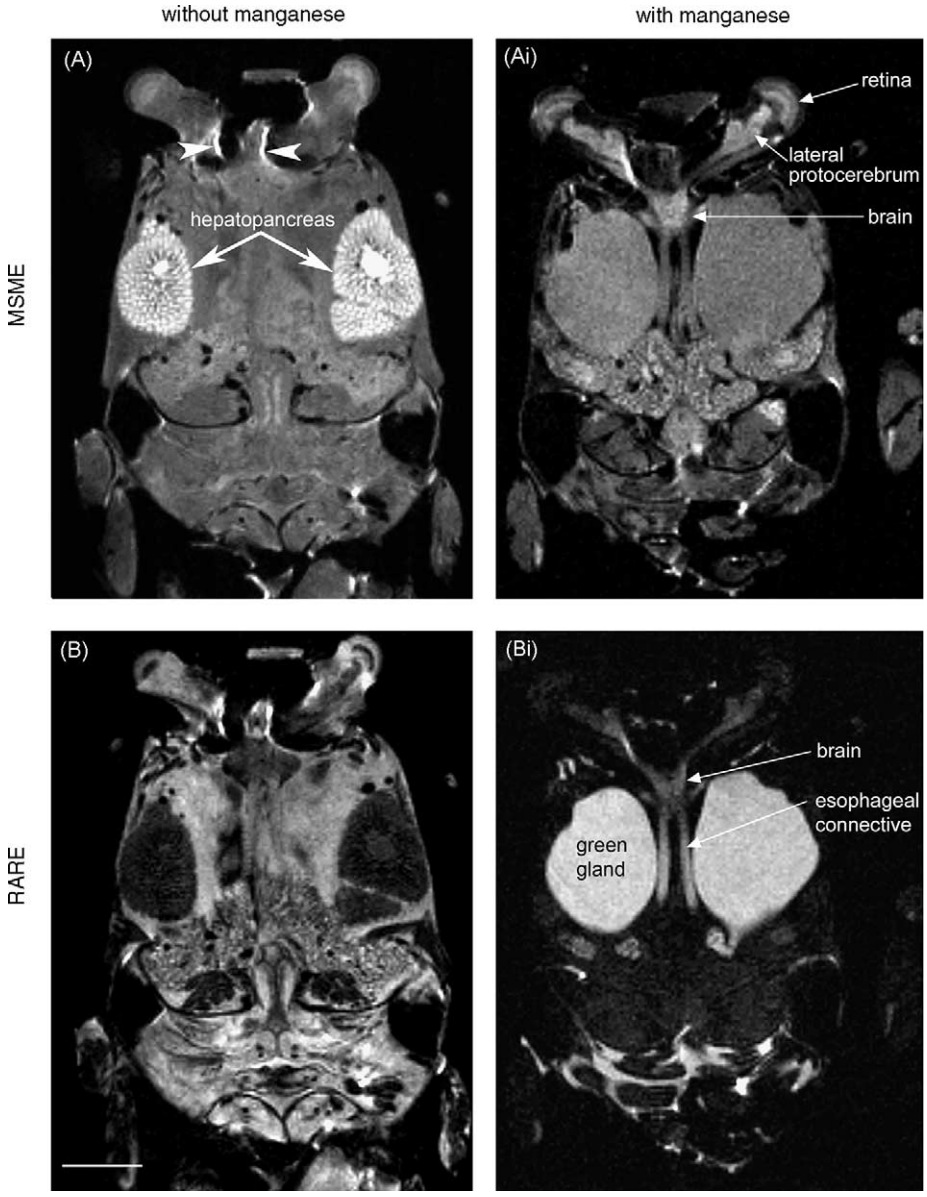

Fig. 3. Effect of Mn^{2+} on visualization of the central nervous system in 300 μm sections acquired with the MSME and RARE protocols. Addition of Mn^{2+} is more effective in enhancing the contrast of neural structures in T1-weighted (MSME; A and Ai) than T2-weighted (RARE; B and Bi) images relative to adjacent tissues, although both MSME and RARE images are enhanced. The lateral protocerebrum (eyestalk ganglia) and brain are more readily resolvable in the T1-weighted than in the T2-weighted Mn^{2+}-enhanced images. Note that (A) and (B) show the same section without Mn^{2+}-enhancement; (Ai) and (Bi) are the same section, taken at a more ventral level than (A) and (B), but with Mn^{2+}-enhancement. Arrowheads in (A) indicate some of the artifacts due to magnetic field inhomogeneities at air–fluid interfaces. (A) (Pre-Mn^{2+}): MSME, FOV 3.2 cm, MTX 256, N_{avg} 8, TR 1310 ms, TE 10.2 ms, TA 26.2 min; (Ai) (post-Mn^{2+}): MSME, FOV 2.9 cm, MTX 256, N_{avg} 3, TR 1010 ms, TE 10.2 ms, TA 12.6 min; (B) (pre-Mn^{2+}): RARE, FOV 3.2 cm, MTX 256, N_{avg} 8, TR 5513 ms, TE 67.5 ms, TA 23.1 min; (Bi) (post-Mn^{2+}): RARE, FOV 2.9 cm, MTX 256, N_{avg} 3, TR 3651 ms, TE 46 ms, TA 5.5 min. Scale bar in (B) = 2.5mm.

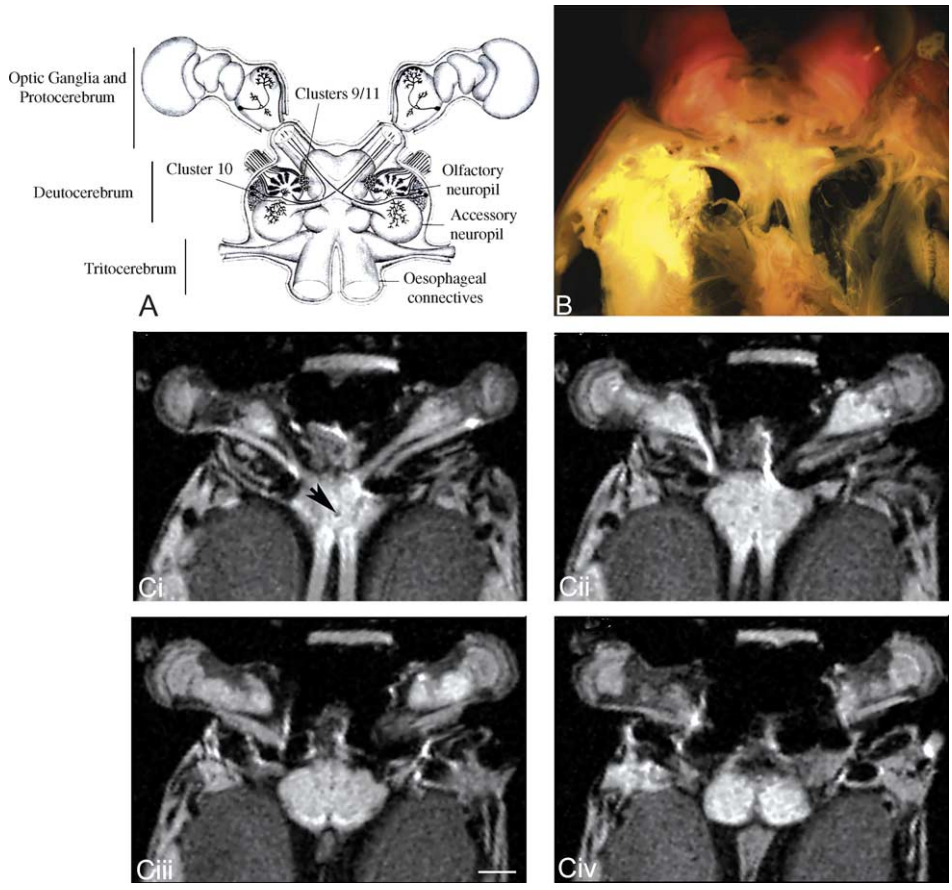

Fig. 4. Visualization of the brain and optic neuropils in serial 300 μm sections using MEMRI and the MSME protocol. (A) Schematic drawing of the brain, including the lateral protocerebrum (eyestalks), and illustrating the major neuropil regions of the deutocerebrum. (B) Fixed neural tissue from *C. destructor*, dissected to reveal the gross anatomy of the brain, eyestalks and nerve roots. (Ci–iv) Serial MRI sections through the brain in the dorsal-ventral plane, illustrating the esophageal connectives, nerve roots and substructures of the brain and eyestalks. Most of these structures are obscured by traditional anatomical preparations (B), unless they are sectioned and stained. Arrow in (Ci) points to the dorsal cerebral artery. MSME, FOV 2.8 cm, MTX 256, N_{avg} 8, TR 1543 ms, TE 10.2 ms, TA 52.4 min. Scale bar in (Ciii) = 1 mm.

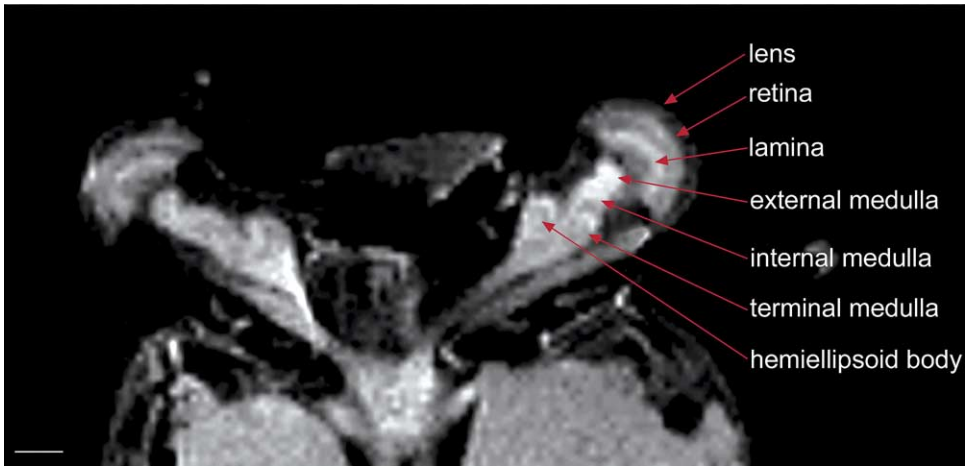

Fig. 5. Individual neuropil regions in the lateral protocerebrum are revealed in this high-resolution 300 μm Mn^{2+}-enhanced image of the eyestalks of *C. destructor* using the T1-weighted MSME protocol. MSME, FOV 2.9 cm, MTX 256, N_{avg} 3, TR 1010 ms, TE 10.2 ms, TA 12.5 min. Scale bar = 1 mm.

areas without detail using the T2-weighted sequence. The brain and neural connectives are evident, although the contrast is low with both protocols.

At a magnetic field strength of 9.4 T, magnetic field inhomogeneities at air–fluid interfaces can cause image artifacts to appear. Such inhomogeneities are apparent, for example, in all frames of Fig. 3 (see white arrowheads, Fig. 3A, for example) as bright narrow lines. Changing the direction of the magnetic field readout gradient changes the direction of these artifacts (images not shown).

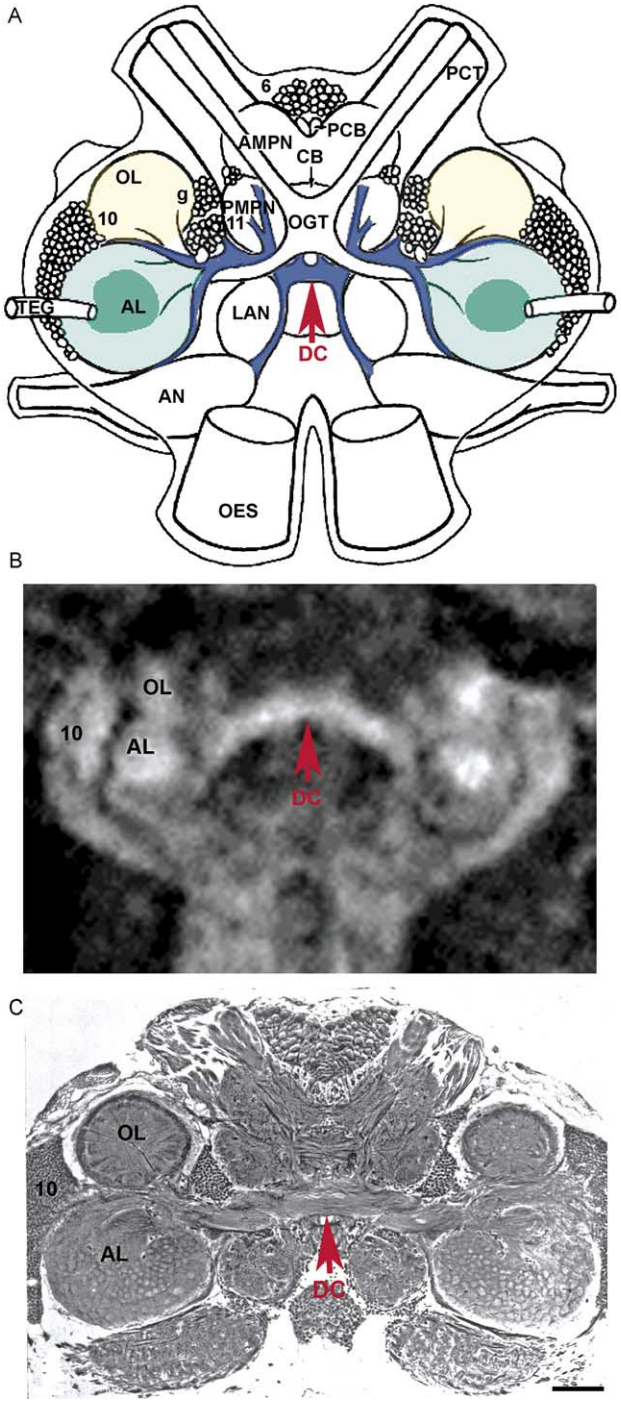

After injection of Mn^{2+}, however, contrast levels in several tissues are altered, and neural tissues are significantly enhanced relative to other tissues, in images acquired using both pulse sequences (compare Fig. 3A and Ai; B and Bi). Slices taken in the same subject and in the same plane using both sequences (Fig. 3Ai and Bi) illustrate that the T1-weighted pulse sequence provides superior contrast for the brain, with TR values ranging from 1000 to 1300 ms. The esophageal connectives, brain, eyestalks and nerves emerging from the brain are apparent in both types of images. In addition, it is possible in T1-weighted images to resolve the dorsal artery in the brain (arrow, Fig. 4Ci, TR = 1543 ms), the lens, retina and individual neuropils in the lateral protocerebrum (lamina, external medulla, internal medulla, terminal medulla and hemiellipsoid body) (Fig. 5, TR = 1010 ms), and neuronal structures within the brain, such as the olfactory and accessory lobes, cell somata and axon tracts in the deutocerebral commissure (Fig. 6B, TR = 300 ms). This level of resolution suggests that it will be feasible to use MRI methods for tract-tracing in the nervous system.

4. Discussion

Two MRI pulse sequences were found to be useful for the crayfish studies: (1) a multi-slice rapid acquisition relaxation-enhanced (fast spin echo) pulse sequence (Bruker ParaVision RARE_BIO) used to produce T2-weighted images and (2) a multi-slice spin echo sequence (Bruker ParaVision MSME_BIO) used to produce T1-weighted images. The application of different pulse sequences may be used to capitalize on the different relaxation times of water protons in

Fig. 6. Mn^{2+}-enhancement of fiber tracts and neuropils in the brain. In this preparation, Mn^{2+} enhances the fibers in the deutocerebral commissure (DC) and the bilateral neuropils to which these project (AL; accessory lobe). (A) Diagram of the neuropils and tracts in the crayfish brain. The DC (red arrow) is highlighted in blue, the ALs in green, and the olfactory lobes (OLs) in yellow. The ALs consist of separate areas (medulla and cortex; Sullivan and Beltz, 2005) shown here in two shades of green. The DC fibers project anteriorly into the median protocerebrum to their cell somata, laterally to the ALs, and posteriorly to the antenna II neuropils (AN) in the tritocerebrum. (B) Mn^{2+}-enhanced MR image of the crayfish brain (500 μm slice thickness) taken in the plane of the DC (red arrow), which is clearly observed extending between the ALs on either side of the brain. The medulla of the AL also is selectively labeled, as are parts of the OLs, located anterior to the ALs. Labeled areas in the region of the cluster 10 cell somata are also evident. MSME, FOV 2 cm, MTX 256, N_{avg} 8, TR 336.7 ms, TE 10.2 ms, TA 11.5 min. (C) Silver-impregnated histological section (from Sandeman and Luff, 1973) in the plane of the deutocerebral commissure showing the DC (red arrow) and its projections to the protocerebrum, tritocerebrum and ALs. *Abbreviations*: AL, accessory lobe; AMPN, anterior median protocerebral neuropil; AN, antenna II neuropil; CB, central body; LAN, lateral antennular neuropil; OGT, olfactory globular tract; OES, esophageal connective; OL, olfactory lobe; PCB, protocerebral bridge; PCT, protocerebral tract; PMPN, posterior median protocerebral neuropils; TEG, tegumentary nerve; numbers refer to cell clusters (Sandeman et al., 1992). Scale bar in C = 100 μm.

specific tissue types, which affect the contrast of a given slice of a sample. In addition, contrast agents that change the relaxation time of the magnetic moments are used to further enhance differences in contrast among different tissue types. In this study, Mn^{2+} ions have been found to be effective for contrast enhancement.

All images shown were acquired in less than an hour with in-plane resolution of $\sim$100 μm × 100 μm and slice thicknesses ranging from 300 to 500 μm. These high resolution, thin slices revealed fine details of the crayfish anatomy previously visible only in histological sections of fixed and stained tissues. Although imaging awake humans or anesthetized animals necessitates the use of much faster imaging sequences, the ability to immobilize the crayfish for many hours at a time with no apparent deleterious effects allows the use of multiple, longer imaging sequences providing the necessary signal-to-noise ratio for these high resolution studies.

MR images reveal features of the anatomy of the crayfish even without Mn^{2+} injection (Fig. 2). The use of T1- and T2-weighted sequences allowed observation of different anatomical features. The stomach, pylorus, blood sinuses, musculature and hepatopancreas are readily identifiable in both T1- and T2-weighted images, although the appearance of these structures varies depending upon the pulse sequence. MR images also show variability in structure and contrast among animals at different stages in their molting and reproductive cycles, even when the same pulse sequence is used (images not shown). This variability highlights the necessity for tightly controlling housing, feeding, time of day of imaging, molt stage, weight and sex, when crayfish are to be used for studies of neural activity.

Mn^{2+} is useful as a contrast agent in living neural tissues because it is paramagnetic and is taken up preferentially in neural tissue (Baden and Neil, 1998) because it mimics Ca^{2+}. For instance, Narita et al. (1990) have shown that Mn^{2+} enters nerve terminals during action potentials through voltage-gated Ca^{2+} channels. Furthermore, Mn^{2+} flow through presynaptic Ca^{2+} channels evokes transmitter release from depolarized nerve endings (Drapeau and Nachshen, 1984). Neural activity therefore continues in regions of the brain containing trace amounts of Mn^{2+}, apparently without impairment, as shown by experiments on murine olfactory function where odors were still detected (Kita et al., 1981; Pautler et al., 1998). However, Mn^{2+} outcompetes Ca^{2+} for binding sites, such that high concentrations of Mn^{2+} can completely inhibit Ca^{2+} uptake. Such preferential uptake of Mn^{2+} is the basis of Mn^{2+} toxicity, resulting in a lack of Ca^{2+} transport to regions of the body where it is needed for metabolism, thereby causing impairment of Ca^{2+}-dependent processes (Aschner and Gannon, 1991). Therefore, for Mn^{2+}-contrast imaging, titration of Mn^{2+} and use of the lowest possible dose are critical. Consistent with studies in mice (Pautler et al., 1998), Mn^{2+} diffuses out of tissues in crayfish over a period of days and is then excreted via the green gland.

Manganese's mimicry of Ca^{2+} in uptake by active neurons and its movement along axons also has provided an approach for neural tract-tracing and the potential for a brain activity assay. Once Mn^{2+} has been taken up by active neurons, it is transported along those neurons, which can then be imaged using MRI over a period of time during the transport process. Such a study was conducted by Pautler et al. (1998), where the projections of olfactory and optic nerves of live mice were traced to their respective regions of the brain. Tjälve et al. (1995) also demonstrated that Mn^{2+} could be used in neural tract-tracing of the olfactory tracts of northern pike fish, revealing the path from the naris to the olfactory bulbs. Likewise, injection of Mn^{2+} into the high vocal center in starlings labeled associated song-control nuclei and allowed an assessment of the volumes of these areas using MRI (Van der Linden et al., 2002). Such Mn^{2+}-based MRI methods provide an alternative to traditional neural tract-tracing methods which make use of dyes or fluorophores. Mn^{2+} travels as fast as the fastest dyes (Leergaard et al., 2003; Pautler et al., 1998; Saleem et al., 2002; Van der Linden et al., 2002; Watanabe et al., 2001), and unlike traditional methods, does not require sacrificing the subject.

Mn^{2+} also has potential as a contrast agent for mapping neural activity related to behavioral patterns. In vertebrate organisms, blood oxygenation level-dependent (BOLD) functional MRI (fMRI) measures changes in hemodynamics (Ogawa et al., 1998). These studies depend on the assumption that areas of the brain with increased activity will experience an increase in oxygenated blood flow. This less direct method of measuring neural activity cannot be used with crustaceans, which possess hemocyanin, neither form of which is paramagnetic. Instead, T1-weighted Mn^{2+}-enhanced MRI (MEMRI) allows visualization of active regions of the brain in a hemodynamic-independent manner wherein neural activity visualized with Mn^{2+}contrast depends directly on active synapses taking up Mn^{2+} at the sites of normal Ca^{2+} influx. A successful application of this method in a study of rats by Lin and Koretsky (1997) showed that brain activation caused by chemical stimulation with glutamate, by lowering the anesthesia dose, and by sensory stimulation, all caused MRI enhancement in the presence of Mn^{2+}. The advantage of MEMRI over traditional fMRI is that one can inject Mn^{2+} into an animal, allow it to perform a behavioral task while the Mn^{2+} is being sequestered in brain regions of high-activity, and then take an MR image of the region of activity.

Although many anatomical features are observed in crayfish without Mn^{2+}, the nervous system is particularly difficult to resolve. Using the T1-weighted pulse sequence, the brain and stomach, which is adjacent to the brain, have similar image intensities; the brain and nervous system are therefore difficult to resolve from surrounding tissues. Images acquired with the T2-weighted sequence have a much greater contrast range; the stomach, hemolymph and pylorus are particularly noticeable, and the brain is distinguishable. However, when $MnCl_2$ is administered and the T1-weighted pulse

sequence is used, the nervous system can be imaged with a level of resolution that allows visualization of the protocerebral tract, esophageal connectives and other nerves emanating from the brain, the dorsal artery in the brain, the layered neuropils of the lateral protocerebrum and eyestalk, and neuropil regions and tracts within the midbrain, or deutocerebrum (Figs. 4–6). This is expected, as Mn^{2+} accumulates preferentially in neural tissues and shortens the T1 values of their water protons. Mn^{2+} therefore provides a degree of contrast enhancement that allows the use of MRI for visualizing neural structures in this non-vertebrate organism, and lays the foundation for further development of Mn^{2+}-enhanced MRI methods.

The ability to resolve fiber tracts in the brain and layers within specific neuropil regions in the brain and lateral protocerebrum (Fig. 5) suggests that the use of these non-vertebrate organisms for neural tract-tracing is an achievable goal. Further, the labeling we observe in the deutocerebrum is highly specific. The accessory lobe, an area that processes higher-order sensory information, has important functional subdivisions (the cortex and medulla) that receive different inputs; the medulla receives primarily visual and tactile inputs (Sandeman et al., 1995), whereas the cortex receives olfactory input (Sullivan and Beltz, 2005). Our MR images resolve these functionally distinct regions and show the AL medulla highlighted relative to the surrounding AL cortex (Fig. 6B). The deutocerebral commissure, which carries the axons of interneurons projecting to the AL, is also hyperintense. These features in combination with contrast in the olfactory lobe itself (Fig. 6B), suggest that neurons involved in the processing of visual and chemosensory inputs have been selectively enhanced. While we do not currently understand the basis for the selective enhancement of these pathways, such images indicate that Mn^{2+} may be differentially accumulated relative to neural activity, suggesting that neural activity mapping in these organisms is feasible. Future experiments will test this possibility with controlled activation of visual or olfactory receptors using natural stimuli, to determine whether or not we can bias the uptake of Mn^{2+} by selectively activating specific sensory pathways.

The present MRI study, which compares the results of different pulse sequences for visualizing tissues in crayfish and the use of Mn^{2+} for imaging neural tissues, sets the stage for the development of tract-tracing and activity-based mapping by MRI in non-vertebrate organisms. It demonstrates that using high magnetic field strengths and powerful gradients allows the acquisition of well resolved, high contrast images in less than an hour. Future experiments will selectively activate specific sensory pathways in crayfish and test the use of Mn^{2+} as both an activity and pathway-selective marker.

Acknowledgements

We thank Joanne Hunter and Sheena Mehta for the MR image shown in Fig. 6B, Jeannie Benton for technical assistance and critical readings of the manuscript, and Pat Carey and Ginny Quinan for animal care. We also thank Jens Herberholz for helpful suggestions on the use of Mn^{2+} in crayfish.

References

Abbott NJ. The organization of the cerebral ganglion in the shore crab, *Carcinus maenas*. II. The relation of intracellular blood vessels to other brain elements. Z Zellforsch 1971;120:401–20.

Abbott NJ. Access of ferritin to the interstitial space of *Carcinus* brain from intracerebral blood vessels. Tissue Cell 1972;4:99–104.

Aoki I, Tanaka C, Takegami T, Ebisu T, Umeda M, Fukunaga M, et al. Dynamic activity-induced manganese dependent contrast magnetic resonance imaging (DAIM MRI). Magn Reson Med 2002;48:927–33.

Aschner M, Gannon M. Manganese neurotoxicity: cellular effects and blood brain barrier transport. Neurosci Biobehav Rev 1991;15:333–40.

Baden SP, Neil DM. Accumulation of manganese in the haemolymph, nerve and muscle tissue of *Nephrops norvegicus* (L.) and its effect on neuromuscular performance. Comp Biochem Physiol A Mol Integr Physiol 1998;119:351–9.

Brinkley C, Kolodny NH, Beltz BS, Sandeman DC, Kohler SJ. Mapping neural activity in *Cherax destructor* using manganese-enhanced magnetic resonance imaging. Int Cong Neuroeth 2004:252.

Burnett KR, Goldstein EJ, Wolf GL, Sen S, Mamourian AG. The oral administration of $MnCl_2$: a potential alternative to IV injection for tissue contrast enhancement in magnetic resonance imaging. Magn Reson Imaging 1984;2:307–14.

Cory DA, Schwartzentruber DJ, Mock BH. Ingested manganese chloride as a contrast agent for magnetic resonance imaging. Magn Reson Imaging 1987;5:65–70.

Drapeau P, Nachshen DA. Manganese fluxes and manganese-dependent neurotransmitter release in presynaptic nerve endings isolated from rat brain. J Physiol 1984;348:493–510.

Fornasiero D, Bellen JC, Richmond JB, Catterton BE. Paramagnetic complexes of manganese(II), iron(III), and gadolinium(III) as contrast agents for magnetic resonance imaging: the influence of stability constants on the biodistribution of radioactive aminopolycarboxylate complexes. Invest Radio 1987;22(4):322–7.

Geraldes CF, Sherry AD, Brown III RD, Koenig SH. Magnetic field dependence of solvent proton relaxation rates induced by Gd^{3+} and Mn^{2+} complexes of various polyaza macrocyclic ligands: implications for NMR imaging. Magn Reson Med 1986;3(2):242–50.

Herberholz J, Mims CJ, Xihang X, Hu X, Edwards DH. Anatomy of a live invertebrate revealed by manganese-enhanced magnetic resonance imaging. J Exp Biol 2004;207:4543–50.

Humason GL. Animal tissue techniques. San Francisco: Freeman and Co. Inc; 1979. p. 14.

Hunter DR, Komai H, Haworth RA, Jackson MD, Berkoff HA. Comparison of Ca^{2+}, Sr^{2+}, and Mn^{2+} fluxes in mitochondria of the perfused rat heart. Circ Res 1980;47:721–7.

Kita H, Narita K, Kloot WV. Tetanic stimulation increases the frequency of miniature end-plate potentials at the frog neuromuscular junction in Mn^{2+}, Co^{2+} and Ni^{2+}-saline solutions. Brain Res 1981;205:111–21.

Leergaard TB, Bjaalie JG, Devor A, Wald LL, Dale AM. In vivo tracing of major rat brain pathways using manganese-enhanced magnetic resonance imaging and three-dimensional digital atlasing. NeuroImage 2003;20:1591–600.

Lin Y, Koretsky AP. Manganese ion enhances T1-weighted MRI during brain activation: an approach to direct imaging of brain function. Magn Reson Med 1997;38:378–86.

London RE, Toney G, Gabel SA, Funk A. Magnetic resonance imaging studies of the brains of rats treated with manganese chloride. Brain Res Bull 1989;23:229–35.

McVean A. Autotomy. In: Sandeman DC, Atwood HL, editors. Neural integration and behavior. In: Bliss De, editor. The biology of crustacea, vol. 4. NY: Academic Press, 1982. p. 107–130.

Michaelis T, Watanabe T, Natt O, Boretius S, Frahm J, Utz S, et al. In vivo 3D MRI of insect brain: cerebral development during metamorphosis of *Manduca sexta*. NeuroImage 2005;24:596–602.

Narita K, Kawasaki F, Kita H. Mn and Mg influxes through Ca channels of motor nerve terminals are prevented by verapamil in frogs. Brain Res 1990;510:289–95.

Newland M, Cox C, Hamada R, Oberdoerster G, Weiss R. The clearance of manganese chloride in the primate. Fundam Appl Toxicol 1987;9:314–28.

Ogawa S, Kim S-G, Ugurbil K, Menon RS. On the characteristics of fMRI in the brain. Ann Revs Biophys Biomol Struct 1998;27:447–74.

Pautler RG, Koretsky AP. Tracing odor-induced activation in the olfactory bulbs of mice using manganese-enhanced magnetic resonance imaging. NeuroImage 2002;16:441–8.

Pautler RG, Silva AC, Koretsky AP. In vivo neuronal tract-tracing using manganese-enhanced magnetic resonance imaging. Magn Reson Med 1998;40:740–8.

Saleem KS, Pauls JM, Augath M, Trinath T, Prause BA, Hashikawa T, et al. Magnetic resonance imaging of neuronal connections in the macaque monkey. Neuron 2002;34:685–700.

Sandeman DC. The vascular circulation in the brain, optic lobes and thoracic ganglion of the crab *Carcinus*. Proc R Soc B 1967;168:82–90.

Sandeman DC, Luff SE. The structural organization of glomerular neuropile in the olfactory and accessory lobes of an Australian freshwater crayfish, *Cherax destructor*. Z Zellforsch 1973;142:37–61.

Sandeman D, Beltz BS, Sandeman R. Crayfish brain interneurons that converge with serotonin giant cells in accessory lobe glomeruli. J Comp Neurol 1995;352:263–79.

Sandeman D, Sandeman R, Derby C, Schmidt M. Morphology of the brain of crayfish, crabs, and spiny lobsters: a common nomenclature for homologous structures. Biol Bull 1992;183:304–26.

Sullivan JM, Beltz BS. Integration and segregation of inputs to higher-order neuropils of the crayfish brain. J Comp Neurol 2005;481:118–26.

Tjälve H, Henriksson J, Tallkvist J, Larsson B, Lindquist N. Uptake of manganese and cadmium from the nasal mucosa into the central nervous system via olfactory pathways in rats. Pharmacol Toxicol 1996;79:347–56.

Tjälve H, Mejare K, Borg-Neczak K. Uptake of manganese in primary and secondary olfactory neurons in pike. Pharmacol Toxicol 1995;77:23–31.

Van der Linden A, Verhoye M, Van Meir V, Tindemans I, Eens M, Absil P, et al. In vivo manganese-enhanced magnetic resonance imaging reveals connections and functional properties of the songbird vocal control system. Neuroscience 2002;112:467–74.

Watanabe T, Michaelis T, Frahm J. Mapping of retinal projections in the living rat using high-resolution 3D gradient-echo MRI with Mn^{2+}-induced contrast. Magn Reson Med 2001;46:424–9.